



# Quasi-biweekly impact of the atmospheric heat source over the Tibetan Plateau on summer rainfall in Eastern China

Meirong Wang<sup>1</sup> · Jun Wang<sup>2</sup> · Anmin Duan<sup>3</sup> · Jing Yang<sup>4</sup> · Yimin Liu<sup>3</sup>

Received: 22 November 2018 / Accepted: 2 May 2019 / Published online: 9 May 2019  
© The Author(s) 2019

## Abstract

We investigated the intraseasonal relationship between the atmospheric heat source over Tibetan Plateau (TP) and summer rainfall in eastern China. A quasi-biweekly oscillation (QBWO) is the common dominant periodicity over both the TP and eastern China. Crucially, the TP heat source QBWO leads rainfall QBWO over its downstream region by 2–8 days. The QBWO over the TP shows a significant eastward propagation. Phase composite further identified the specific propagation pathway: TP QBWO first propagates eastward to central China, southward to southern China, and then northeastward to the lower reaches of the Yangtze River with a zigzag propagating pathway. Mechanistically, the eastward propagation of the upper level divergence caused by the movement of the 200 hPa jet core and south Asian high contributes to the eastward propagation of the rainfall QBWO. Simultaneously, the eastward (westward) shift in the western north Pacific subtropical high causes deepening (flattening) of the monsoon trough and the occurrence of an anomalous cyclone (anticyclone) over the western north Pacific. An anomalous anticyclonic (cyclonic) circulation around the TP appears with the wet-to-dry (dry-to-wet) phase transition of the TP QBWO. Together, they play a crucial part in the southward (northeastward) movement of the QBWO. Further dynamic analysis indicates that the horizontal moisture advection acts on the whole eastward-propagating process of the QBWO, whereas the horizontal vorticity advection is only significant when QBWO is over the TP. This study shows that the fluctuations in TP heat source are important indicators in extended forecasts of summer rainfall in eastern China.

**Keywords** TP · Atmospheric heat source · Quasi-biweekly oscillation · Intraseasonal variation of precipitation · Atmospheric circulation

✉ Meirong Wang  
wmr@nuist.edu.cn

✉ Jun Wang  
wangjun@nju.edu.cn

<sup>1</sup> Joint Center for Data Assimilation Research and Applications/Key Laboratory of Meteorological Disaster, Ministry of Education/Joint International Research Laboratory of Climate and Environment Change (ILCEC)/Collaborative Innovation Center ON Forecast and Evaluation of Meteorological Disasters, Nanjing University of Information Science and Technology, Nanjing, China

<sup>2</sup> International Institute for Earth System Science, Nanjing University, Nanjing, China

<sup>3</sup> State Key Laboratory of Numerical Modeling for Atmospheric Sciences and Geophysical Fluid Dynamics, Institute of Atmospheric Physics, Chinese Academy of Sciences, Beijing, China

<sup>4</sup> State Key Laboratory of Earth Surface Processes and Resource Ecology (ESPRE)/Academy of Disaster Reduction and Emergency Management Ministry of Civil Affairs and Ministry of Education, Faculty of Geographical Science, Beijing Normal University, Beijing, China

## 1 Introduction

The Tibetan Plateau (TP) is a huge heat source in the summer months and directly heats the mid-troposphere, regulating both the weather and climate throughout the northern hemisphere (Flohn 1957, 1960; Luo and Yanai 1983, 1984; Wu and Zhang 1998; Duan and Wu 2005; Wu et al. 2012). Numerous studies (Tao and Ding 1981; Hsu and Liu 2003; Duan and Wu 2005; Mao and Wu 2006; Duan et al. 2013; Hu and Duan 2015) have shown that there is a close connection between the atmospheric heat source over the TP and summer precipitation in eastern China.

The TP has been identified as an active center of intraseasonal variability (ISV) in mid-latitudes, with significant ISV modes in a number of meteorological elements (Nitta 1983; Xie et al. 1989; Krishnamurti and Subrahmanyam 1982; Zhang et al. 2014, 2009a, b; Yang and Li 2017; Yang et al. 2018). Nitta (1983) found that the total heating, precipitation and relative vorticity over the eastern TP in 1979 showed

medium-period fluctuations with 10-, 15- and 30-day cycles. Fujinami and Yasunari (2001, 2004, 2009) systematically analyzed the ISV changes over and around the TP and suggested that the 7–20-day convective variability over the TP is associated with mid-latitude waves. A similar result was also reported by Hu et al. (2016). Oscillations with cycles of 20–30, 14 and 8 days were detected over the TP during the summer of 1998 (Yamada and Uyeda 2006; Zhang et al. 2014). Based on long-term observations and reanalysis datasets, several studies have suggested that multiscale ISV modes exist over TP and a quasi-biweekly oscillation (QBWO) is dominant (Wang and Duan 2015; Wang et al. 2017, 2018; Yang et al. 2017).

The ISV over the TP has influences on local and large-scale weather systems, such as the subtropical high (Li et al. 1991), the South Asian high (Liu and Lin 1991), the weather events (Yasunari and Miwa 2006; Fujinami and Yasunari 2009) and the plateau low vortex (Zhang et al. 2014). Yasunari and Miwa (2006) found a relationship between the rainfall/cloud systems and QBWO over the TP and eastern China regions in 1998 that was one of active QBWO year over the TP. Fujinami and Yasunari (2009) showed that QBWO related to the TP can affect the meridional (southward) movement of Meiyu front and northeastward movement of synoptic-scale low over the Meiyu front. The atmospheric QBWO has a strong modulating effect on the diurnal variation of the occurrence frequency of TP vortices (Li et al. 2017). In addition, several vortices moving off the plateau have significant QBWO features and the QBWO in the atmospheric circulation and heating fields have major impacts on the eastward movement of these vortices (Li and Zhang 2018). The oscillations over the TP can also affect the mean summer rainfall, both on the TP and in eastern China. Zhou et al. (2000) suggested that the ISV characteristics of the sensible heat flux and zonal winds are consistent with the behavior of summer rainfall in the local region and in northern China. An apparent association was found between the changes in the low-frequency heat source over the TP and droughts and floods in the Yangtze–Huaihe river basin in 2001 and 2003 (Gong et al. 2007). In terms of the ISV of the summer rainfall, Wang et al. (2009) detected a relationship between the atmospheric heat source over the TP and rainfall in the middle and lower reaches of the Yangtze River. They found that the heat source over the TP was significantly correlated with the summer rainfall in 1978 on a 10–20-day timescale, whereas the same correlation was seen on a 30–60-day timescale in 1999.

The ISV over East Asia is strongly correlated with extreme precipitation (Yang 2009). Understanding the ISV of rainfall provides a crucial theoretical basis for solving the challenge of medium- and long-term forecasts (Kikuchi and Wang 2009; Lau 2002). Many studies have considered the linkage between the seasonal mean heat source over the

TP and drought and flood conditions in East Asia, whereas the influence of the ISV of the TP heat source on the ISV of summer rainfall in East Asia has received less attention, particularly with regard to its mechanisms. Previous research has focused mainly on case studies and local areas due to the lack of observational datasets. Our purpose was to determine the impact of the heat fluctuations in the atmosphere over the TP on the summer rainfall ISV in eastern China based on long-term observations and reanalysis datasets, including identifying the regions affected, the specific pathways and possible mechanisms.

This paper is organized as follows. Section 2 presents the data and methodology. Section 3 presents the characteristics of the ISV over the TP and eastern China. Section 4 investigates the impact of the atmospheric QBWO over the TP on the ISV of summer rainfall in eastern China and the related circulation and physical fields. We illustrate the specific internal atmospheric dynamic mechanisms during the eastward-propagating process in Sect. 5. A summary and discussion are provided in Sect. 6.

## 2 Data and methods

### 2.1 Dataset

We used the daily high-resolution ( $0.5^\circ \times 0.5^\circ$ ) precipitation dataset from the China Meteorological Administration for the time period 1979–2014 (Zhao and Chen 2001). Other observational variables from 71 stations across the TP were used to calculate the sensible and latent heat fluxes over the TP. We also used the ISCCP (<http://isccp.giss.nasa.gov/projects/flux.html>) and GEWEX-SRB ([http://eosweb.larc.nasa.gov/PROD-OCS/srb/table\\_srb.html](http://eosweb.larc.nasa.gov/PROD-OCS/srb/table_srb.html)) satellite radiation datasets for the time period 1984–2007. Daily atmospheric circulation data were extracted from the Japanese 55-year Reanalysis (JRA-55; Kobayashi et al. 2015) and the European Centre for Medium-Range Weather Forecasts Interim Reanalysis (ERA-Interim; Dee et al. 2011) datasets for 1979–2014, which have horizontal resolutions of  $1.25^\circ \times 1.25^\circ$  and  $1.5^\circ \times 1.5^\circ$ , respectively.

### 2.2 Methodology

#### 2.2.1 Atmospheric heat source

The vertically integrated atmospheric apparent heat source ( $\langle Q_1 \rangle$ -ERA-Interim and  $\langle Q_1 \rangle$ -JRA55) was derived from the ERA-Interim and JRA-55 reanalysis datasets by residual budget analyses (Yanai 1961; Yanai et al. 1973):

$$c_p \left[ \frac{\partial T}{\partial t} + \vec{v} \cdot \nabla T + \left( \frac{p}{p_s} \right)^k \omega \frac{\partial \theta}{\partial p} \right] = Q_1$$

$$\langle Q_1 \rangle = \frac{1}{g} \int_{100}^{P_s} Q_1 dp$$

where  $T$  is temperature,  $\vec{V}$  is the horizontal wind vector,  $p_s$  is the surface pressure,  $p$  is the pressure, and  $k = R/c_p$ ;  $R$  and  $c_p$  indicate the gas constant and specific heat of dry air at constant pressure, respectively.  $\theta$  is potential temperature,  $\omega$  is the vertical velocity.

In comparison, based on the method reported by Duan and Wu (2008) and Wang et al. (2011), the observational atmospheric heat source over the central and eastern TP (E-SRB and E-ISCCP) was calculated based on data from 71 meteorological stations (Fig. S1a) and two satellite radiation datasets (GEWEX-SRB and ISCCP) according to the energy budget formula:

$$E = SH + LH + RC$$

where  $E$  indicates the heat source,  $SH$  is the sensible heat flux,  $LH$  is the latent heat released by rainfall and  $RC$  is the net radiation flux of the air column, which is calculated from the GEWEX-SRB and ISCCP datasets.

### 2.2.2 Power spectral analysis and data filtering

The major periodicity was determined from the mean power spectrum, which is the average of the individual power spectra from the ISV component for each summer during the time period 1979–2014. The significance of the mean power spectrum was tested based on the mean red noise using the method of Gilman et al. (1963).

We used the method of Yang et al. (2009) to obtain the ISV component in the power spectral analysis by: (1) calculating the climatology via climatological 5-day running mean time series; (2) removing the climatology from the raw daily data; and (3) applying a 5-day running mean to remove synoptic fluctuations.

Using the Lanczos filtering method (Duchon 1979), we obtained the 10–20-day signals from the raw dataset. Considering that the degrees of freedom of the filtered data are much less than the sample number, we recalculated the effective degrees of freedom according to the approach of Bretherton et al. (1999).

### 2.2.3 Phase composite analysis

Following the method of Mao and Chan (2005), we applied phase composite analysis to detect the temporal evolution and spatial structure of the ISV. We separated one cycle of ISV into eight phases. Phases 1 and 5 were the maximum (peak positive) and minimum (peak negative) phases, respectively. Phases 2, 4, 6 and 8 indicated the positions at which the cycle was at half its maximum or minimum

value. Phase 3 was the transition from the positive to negative phases and phase 7 was the transition from the negative to positive phases.

## 3 Characteristics of the ISV of the TP heat source and rainfall in eastern China

In order to determine which the vertically integrated atmospheric apparent heat source calculated from the ERA-Interim and JRA-55 reanalysis datasets can better represent the atmospheric heat source over the TP. We first compare their summer mean variations (Fig. S1b). The clear mismatch between E-ISCCP and E-SRB datasets suggests that there are large uncertainties in the radiation data from different satellites. The heat sources from the four datasets show similar interannual variations (Table S1), however, different amplitudes of the trend (Fig. S1b). The  $\langle Q_1 \rangle$ -JRA55 and E-SRB datasets show more consistent variations both in the interannual and trend (Table S1 and Fig. S1b). We also present their intraseasonal variations between  $\langle Q_1 \rangle$ -JRA55 and E-SRB in 3-year samples (Fig. 1). It shows obviously consistent variations with their correlation coefficients of 0.8, 0.87 and 0.86 in 1984, 1997 and 2002, respectively. The mean correlation coefficient can reach 0.69 for total 24 years. We therefore used the  $\langle Q_1 \rangle$ -JRA55 dataset (referred to hereafter as  $\langle Q_1 \rangle$ ) to investigate the ISV of the TP heat source, owing to the limited observations in E-SRB.

Figure 2a firstly shows the spatial distributions of the climatological summer mean  $\langle Q_1 \rangle$  during the period of 1979–2014, suggesting that the whole TP and its surrounding area is mainly covered with uniformly positive heating, with big value center in southern slope of the TP. The heat source is composed of SH, RC and LH, in which the LH released

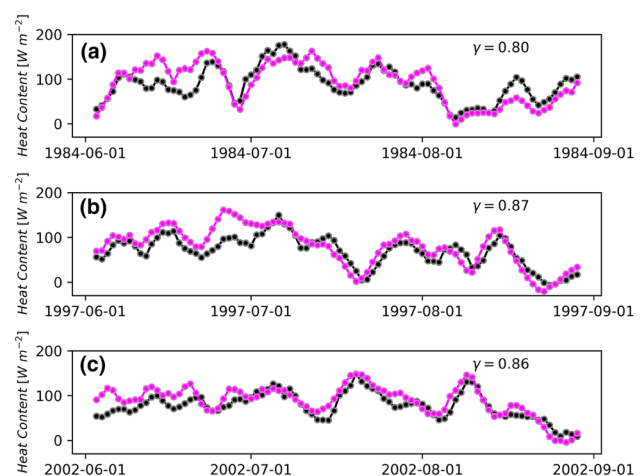


**Fig. 1** Time series of 5-day running average E-SRB (black line) and  $\langle Q_1 \rangle$ -JRA55 (pink line) ( $W m^{-2}$ ) during summer seasons for 3-year samples. The correlation coefficients are also presented as  $\gamma$

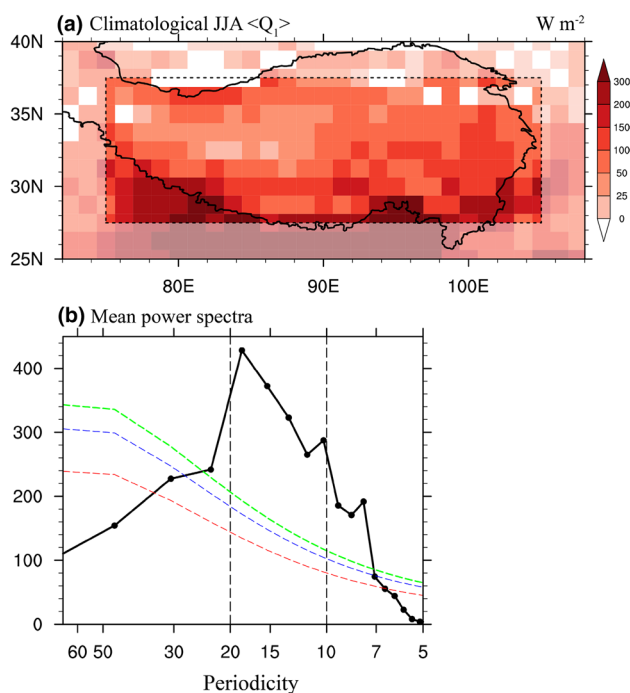


**Fig. 2** **a** Spatial distributions of the summer mean vertical integrated atmospheric apparent heat source ( $W m^{-2}$ ) based on JRA-55 reanalysis data ( $\langle Q_1 \rangle - JRA55$ ) from 1979 to 2014, and the square area ( $75\text{--}105^\circ E$ ,  $28\text{--}38^\circ N$ ) is used to calculate the average heat source over the TP region. **b** Mean power spectra of the TP heat source for the 33 summer seasons during the period 1979–2014. The red dashed line represents the Markov red noise spectrum and the blue and green dashed lines indicate the prior and posterior 99% confidence bounds, respectively. The  $x$  and  $y$  axes show the periodicity and variance, respectively

by rainfall in summer accounts for a significant proportion, with similar spatial distribution of summer mean rainfall in TP region shown in Fig. S2. Therefore, the heat source represents a complex and comprehensive TP heat condition. To examine the dominant periodicity of the atmospheric element over the TP, the power spectra were calculated for daily  $\langle Q_1 \rangle$  anomalies averaged over ( $75\text{--}105^\circ E$ ,  $28\text{--}38^\circ N$ ), for each summer (June–August) from 1979 to 2014. Figure 2b shows the mean power spectra of 36 summer seasons. The 10–20-day oscillation, with a peak at 18 days, is the most dominant frequency band, and has also been reported previously in various meteorological fields (Wang and Duan 2015; Yang et al. 2017; Wang et al. 2018). Another significant band in Fig. 2b is the 7–9-day oscillation.

An empirical orthogonal function (EOF) analysis by calculating a correlation matrix was used to detect the spatial pattern in the summer mean rainfall anomalies in eastern China. Figure 3a shows the first leading EOF mode with an explained variance of 16%. Figure 3a shows a positive rainfall anomaly in southern China ( $100\text{--}120^\circ E$ ,  $22\text{--}28^\circ N$ ) and a negative signal in central China ( $100\text{--}120^\circ E$ ,  $28\text{--}36^\circ N$ ) with

a seesaw pattern. The mean power spectra in Figs. 3b and c show the periodicities for these two regions. The common significant periodicities are clearly 10–20 and 7–9 days and a quasi-30-day oscillation is also robust in the south. We conducted an EOF analysis for the 10–20-day filtered summer rainfall (Fig. S3), which showed a similar pattern to that in Fig. 3a, suggesting that the 10–20-day oscillation is an important factor in the summer rainfall in eastern China.

## 4 Impact of the TP heat source QBWO on the rainfall QBWO in eastern China

### 4.1 Linkage between TP heat source and downstream rainfall on the QBWO timescale

In terms of the common dominant intraseasonal periodicity over the TP and eastern China, we focus here on the QBWO timescale to examine the connection between the TP heat source and the rainfall downstream. Figure 4 shows the spatial correlation coefficients for the TP heat source leading the 10–20-day filtered summer rainfall. The TP heating is closely related to both the rainfall in the local area and in most other parts of China on the QBWO timescale. This phenomenon is not only contemporaneous (Fig. 4a), but also exists when the TP heat source leads the rainfall by about 2–8 days (Fig. 4b–e), suggesting that the QBWO of the TP heat source can serve as an important indicator in forecasting the sub-seasonal variations in rainfall over the TP and its downstream regions. For instance, when the filtered TP heating leads the filtered rainfall by 2 days, robust positive correlation coefficients are located over the whole TP and central China and negative correlation coefficients over southern China—that is, when the TP heat source QBWO is strong, we can predict that more rain will fall over the TP and central China 2 days later, but less rain will fall in southern China. Figure 4 also shows that the areas of significant correlation are constantly changing, especially the regions with a positive correlation (Fig. 4a–c), and that these areas appear to be moving eastward.

We examined the zonal propagation of the QBWO over the TP (Fig. 5) and found that the QBWO over the TP first moves rapidly eastward from the western TP to the eastern TP with a mean speed of about  $6 m s^{-1}$ . After leaving the TP, the QBWO propagates much slower at a speed of about  $3 m s^{-1}$ .

To further understand the variations in the QBWO in rainfall associated with different QBWO phases over the TP, we separated the QBWO cycle of heating over the TP into eight phases and then studied the composite evolution of the 10–20-day filtered rainfall in these eight phases (Fig. 6). In phase 1, an extensive positive rainfall QBWO covers the TP

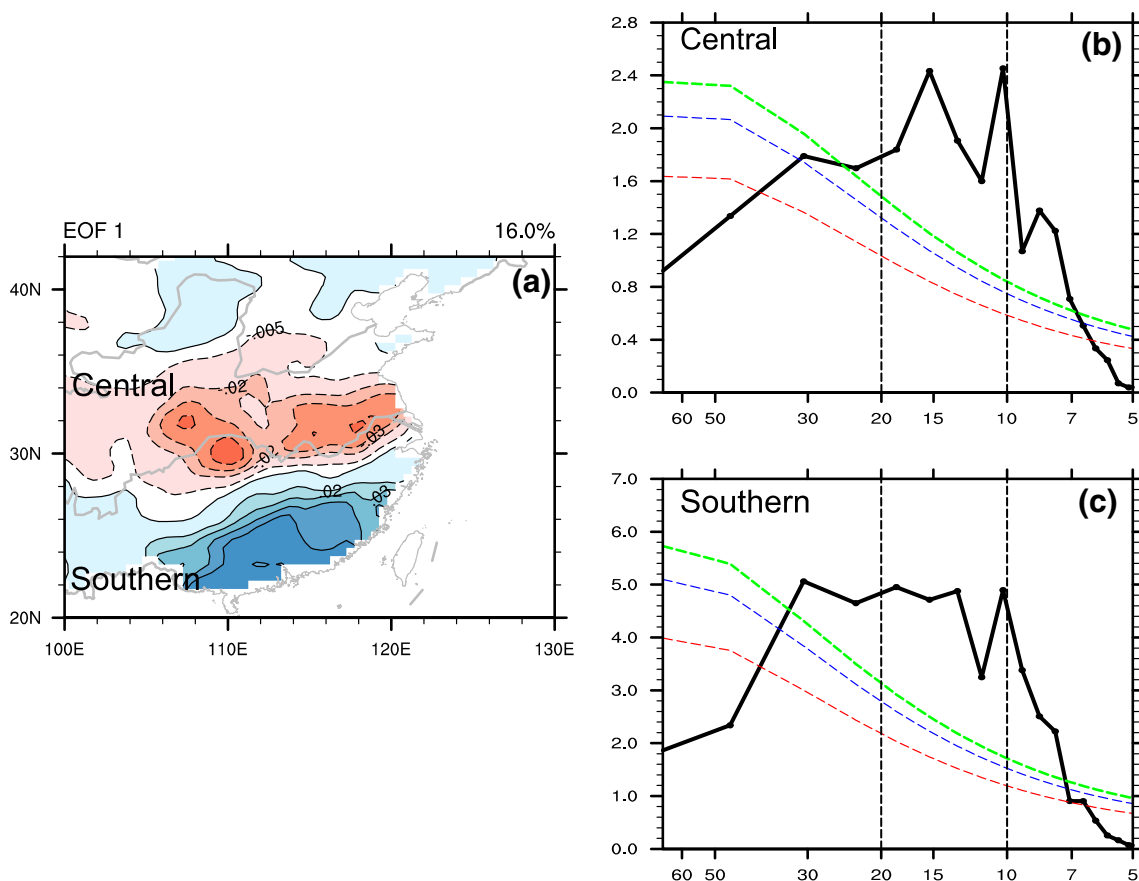


**Fig. 3** **a** The first leading EOF mode of non-filtered summer rainfall ( $\text{mm day}^{-1}$ ) in eastern China between 1979 and 2014 based on observational data. The variance explained by the mode is marked at the upper right of the panel. Mean power spectra of the summer rain-

fall in **b** central ( $100\text{--}120^\circ\text{E}$ ,  $28\text{--}36^\circ\text{N}$ ) and **c** southern ( $100\text{--}120^\circ\text{E}$ ,  $22\text{--}28^\circ\text{N}$ ) China for the 33 summer seasons during the period 1979–2014

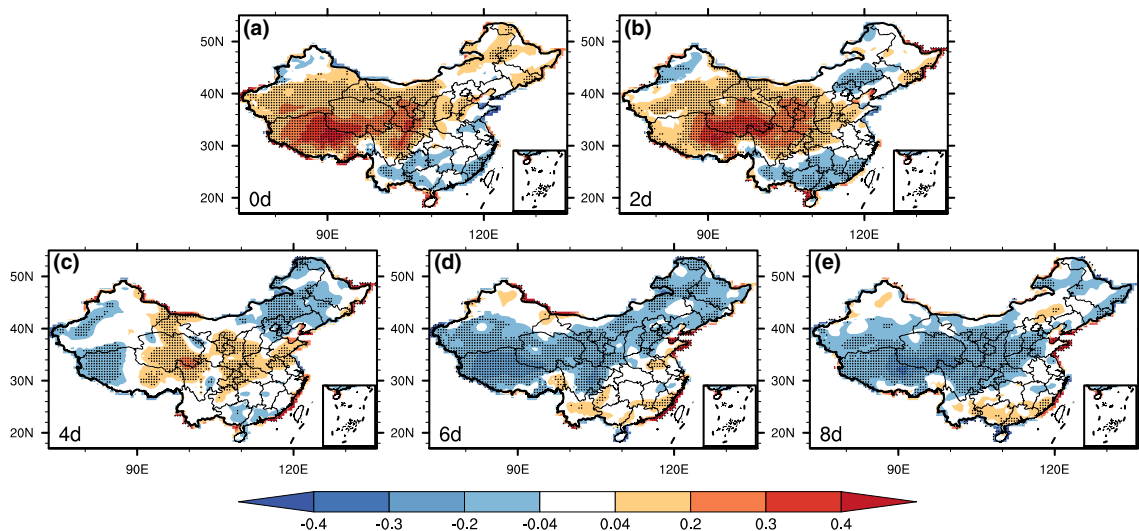


**Fig. 4** Lead correlation coefficient fields between the filtered  $\langle Q_1 \rangle$  dataset over the TP and the filtered summer rainfall. The number 0d at the left corner of the figure shows that  $\langle Q_1 \rangle$  over the

TP and the rainfall in China are contemporaneous. The rest of the numbers indicate the days that  $\langle Q_1 \rangle$  leads the rainfall

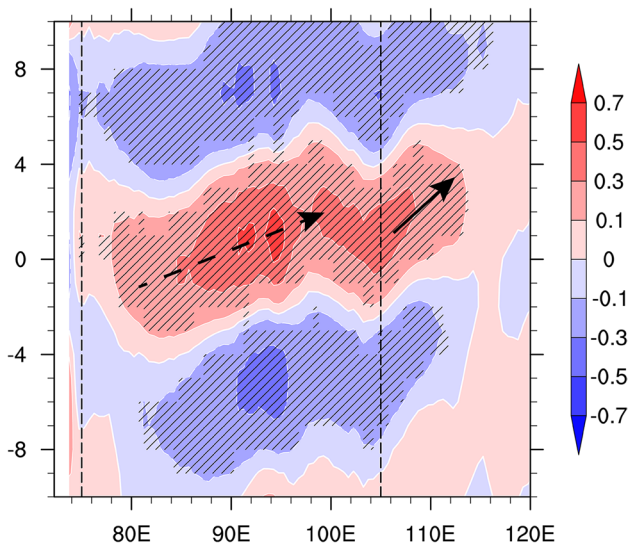


**Fig. 5** Zonal propagation of the filtered summer rainfall averaged along 28–38°N computed from the lead-lag correlation with respect to the heat source averaged over the TP. The unit of the y axis is days. Shading areas denote correlation above the 90% confidence level. The two dashed lines indicate the range of the TP. The black arrows represent the direction of propagation of the QBWO from the TP to its downstream regions

and its eastern lower reaches (110°E), with one large center at 91°E and another at 106°E. The positive QBWO signals propagate gradually eastward and control the whole eastern TP and central China in phase 2. The eastward propagation then weakens and turns southward during phases 3–5. The QBWO signals originating from the TP ultimately arrive in southern China in phase 6 and mix with the signals on the southeastern coast of China, which gradually increase from phases 3–5. However, instead of remaining in southern China, the signals then move northeastward, with a significant large rainfall center in the lower reaches of the Yangtze River in phase 8. The entire propagation process is similar for the negative QBWO signals and the evolution of the positive and negative signals is repeated. Therefore, this propagation of the QBWO in rainfall is clear and significant under the different phases of TP QBWO and shows a zigzag pathway.

We also examined the evolution of the 10–20-day filtered integrated moisture flux transport and divergence (Fig. 7). In phase 1, the robust moisture convergence corresponding to the positive rainfall center (phase 1 in Fig. 6) occurred over the TP and its eastern neighboring areas, closely related to the sustained transport of water vapor by the strong southwesterly flow. The QBWO signals in the moisture convergence center begin to move eastward in phase 2. During phases 3–5, the southwesterly flow on the eastern and southern TP disappears and the anomalous northeasterly airflow is seen. An anomalous cyclone emerges with its center

gradually moving from the western north Pacific (approximately at 23°N, 123°E) to the South China Sea (approximately at 23°N, 116°E). The anomalous northerly airflow prevails to the west of the anomalous cyclone, and it contributes to the southward penetration of the anomalous water vapor as well as moisture convergence (phases 3 and 4). In phase 5, the reinforced moisture convergence occurs over the southern China and South China Sea under the control of the anomalous cyclone, well corresponding to the enhanced anomalous rainfall in phase 5 (Fig. 6). From phases 6–8, the anomalous cyclone vanished, and instead the anomalous anticyclone is established over the western north Pacific and South China Sea. Similarly, the southwesterly flows around the TP and to the west of the anomalous anticyclonic center play important parts in the northeastward propagation of the areas of convergence associated with the QBWO. In sum, the propagation of the anomalous moisture convergence accords well with the evolution of the rainfall anomalies, showing the zigzag pathway.

## 4.2 Large-scale circulation fields related to the QBWO

To better understand how the QBWO of the TP heat source influences the QBWO of rainfall in East Asia, we further investigate the evolution of the large-scale circulation related to the QBWO.

### 4.2.1 Upper tropospheric circulation

Figure 8 shows that the evolution of the 200 hPa divergence in the QBWO anomaly is almost identical to the rainfall patterns in Fig. 6, with the upper level divergence center matching the positive rainfall anomalies. This favors the generation or maintenance of active rainfall.

Figure 8 also shows the 200 hPa raw zonal wind field. The subtropical westerly jet stream (SWJS) is located over East Asia along 40°N, with the jet core moving eastward from about 95°E in phase 1 to 110°E in phase 4. In addition, compared with Fig. 6, it is easy to see that the QBWO in the positive rainfall is always located on the right-hand side of the upper level jet entrance. This is because the right-hand region of the jet entrance is controlled by divergence and updraft. Hence the strong, eastward-propagating jet core leads the QBWO in positive rainfall moving eastward from phases 1–4. In the subsequent phases, the jet core continues moving eastward, while the QBWO in rainfall mainly experiences meridional movement. This means that the SWJS is mainly responsible for the eastward movement of the positive QBWO signals from the TP to central China. Regarding the propagation of the negative rainfall in phases 5–8, a new jet core appears in the north of the TP and then moves eastward. The QBWO in the negative rainfall (Fig. 6) is located

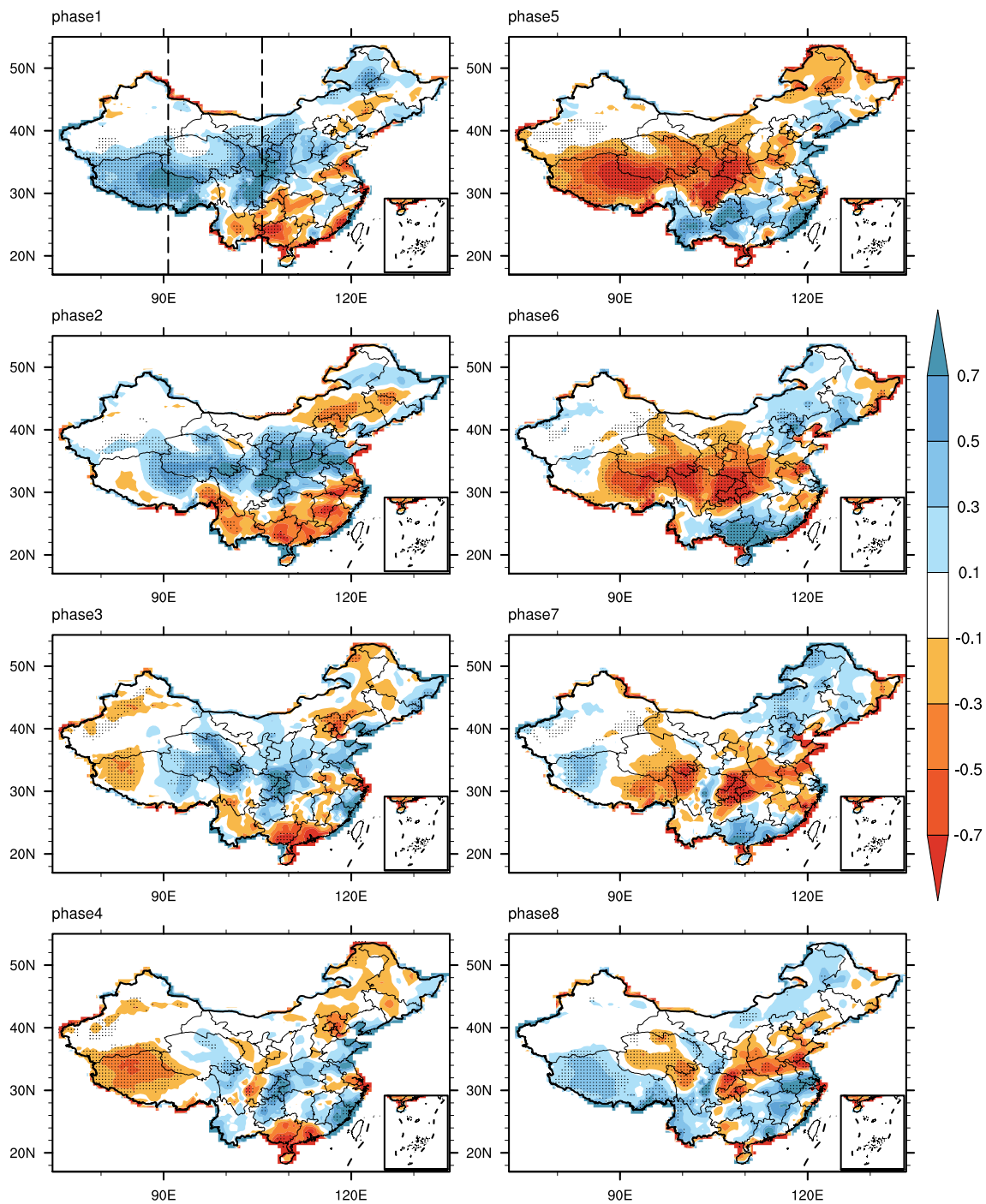


**Fig. 6** Composite evolution of the 10–20 day filtered summer rainfall ( $\text{mm day}^{-1}$ ) during one QBWO cycle of the  $\langle Q_1 \rangle$  over the TP for phases 1–8. The dotted areas are statistically significant at the 90%

confidence level. The dashed lines in phase1 represent the first and the second rainfall centers, respectively

to the right-hand side of the upper level jet exit zone controlled by convergence and downdrafts, which suppress the occurrence and development of rainfall. The characteristics of the eastward propagation of the QBWO in the positive and negative rainfall are almost opposite; both are affected by the SWJS, but in the entrance and exit regions, respectively.

The large upper level system of the South Asian high is also illustrated in Fig. 8. The eastern edge of the South Asian high clearly moves eastward during phases 1–4, from roughly 118 to 128° E. The South Asian high strengthens and enhances the upper level divergence over East Asia, which further helps the eastward propagation of the

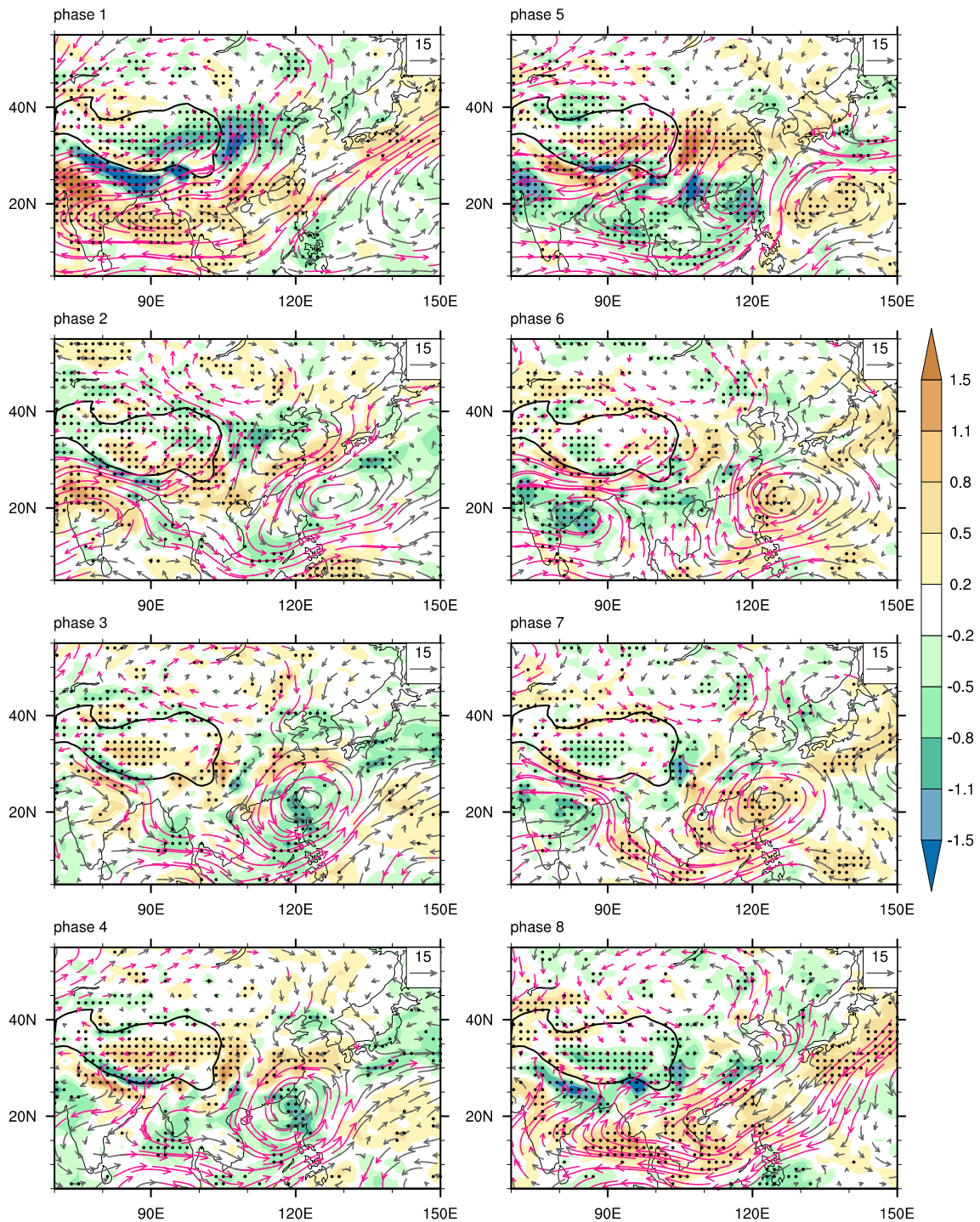


**Fig. 7** As in Fig. 6, but for the 10–20-day filtered integrated water vapor flux (vectors,  $\text{kg m s}^{-1}$ ) and divergence (shaded,  $10^{-5} \text{ kg m}^{-2} \text{ s}^{-2}$ ). The pink vectors exceed the 90% confidence level

positive rainfall in the QBWO anomaly. The clear retreat of the South Asian high corresponds well to the eastward movement of the QBWO signals in the negative rainfall

from the TP in phases 5 and 6, which is almost completely opposite to the movement in phases 1 and 2. The South Asian high remains almost the same in phases 7 and 8.



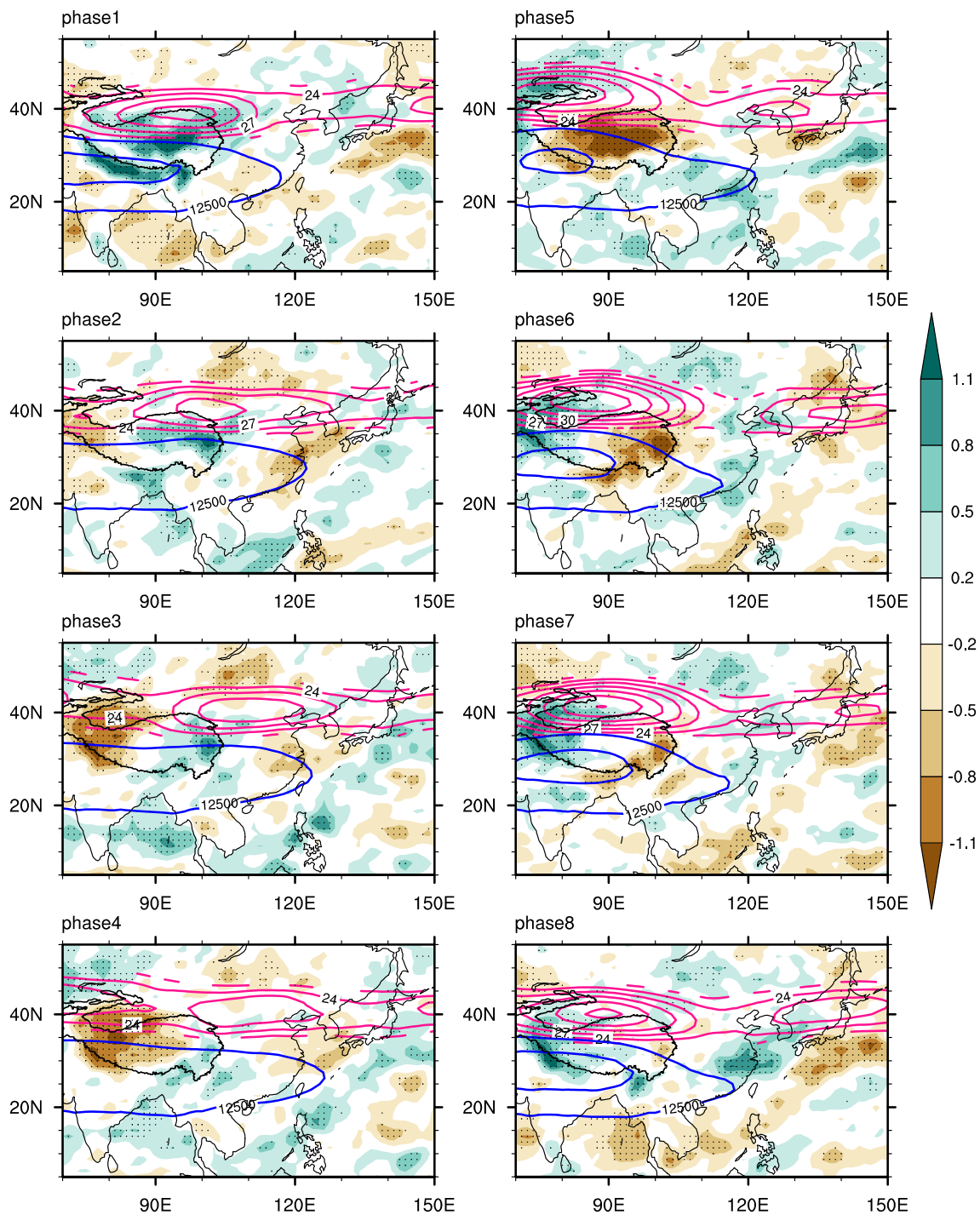


**Fig. 8** As in Fig. 6, but for the 10–20-day filtered divergence (shaded,  $10^{-6} \text{ s}^{-1}$ ), non-filtered zonal wind (pink contour,  $\text{m s}^{-1}$ ) and geopotential height (blue contour, gpm) at 200 hPa

### 4.2.2 Mid- and lower tropospheric circulation

We investigated the changes in circulation associated with the meridional propagation of the rainfall QBWO signals during phases 5–8 in Fig. 6. The related circulation fields

in the mid- and lower troposphere are shown in Fig. S4 and Fig. 9, respectively. The cyclonic circulation controls the TP (Fig. S4) and its surroundings (Fig. S4 and Fig. 9) from phases 1–3, with a southwesterly flow prevailing in the southern and eastern TP, which is consistent with the flow of

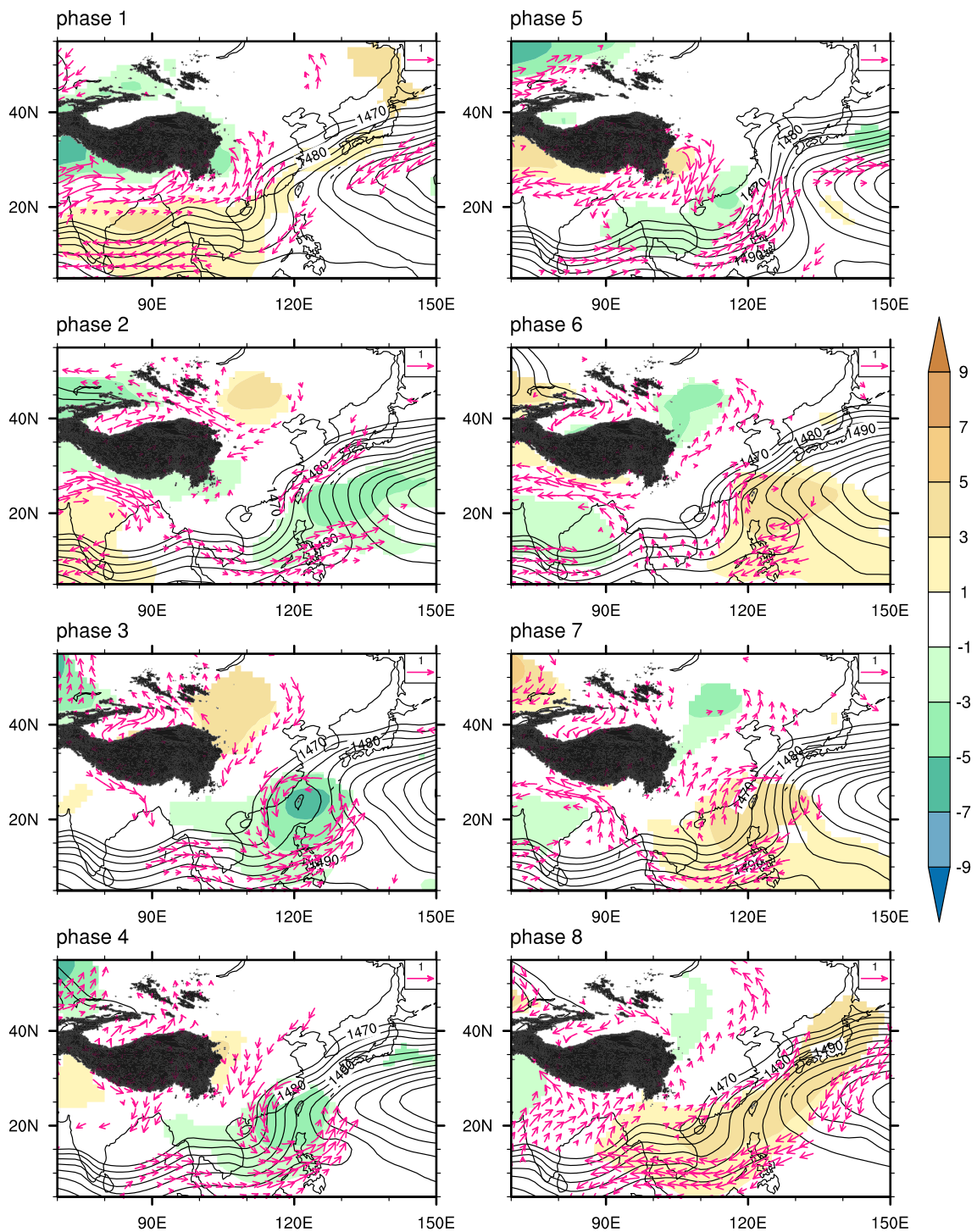


**Fig. 9** As in Fig. 6, but for the 10–20-day filtered geopotential height (shaded, gpm) and wind field (vector,  $\text{m s}^{-1}$ ), and non-filtered geopotential height (contour, gpm) at 850 hPa. The pink vectors exceed the 90% confidence level

the moisture flux shown in Fig. 7. The strong southwesterly wind supplies abundant moisture for rainfall and favors its eastward movement on the QBWO timescale.

Figure 9 shows the significant variation in the western north Pacific subtropical high (WNPSH) for QBWO phases

1–8 over the TP. The WNPSH retreats eastward in phases 2 and 3, contributing to the intensification of the monsoon trough over the western north Pacific and the South China Sea—for example, the 1490 gpm contour moves eastward and extends to the east of the Philippines. Consequently,

a negative anomaly in the geopotential height QBWO and a matching anomalous cyclone occur in the western north Pacific and gradually strengthen, contributing to the southward propagation of the rainfall QBWO signals and the formation of local rainfall over the southeastern coast of China (phases 3–5 in Fig. 6). Another, a dry phase occurs over the TP after the eastward movement of rainfall (phase 5), forming an anomalous anticyclone with northerly winds to the east of the TP. These two processes cause the southward penetration of the anomalous water vapor and moisture convergence (Fig. 7), associated with the change in the location of the rainfall in the QBWO anomaly from phases 3–5. During the following phases (phases 6–8), with the WNPSH shifting farther westward, the negative QBWO in geopotential height is replaced by a positive QBWO (Fig. S4). The monsoon trough then flattens and an anticyclone replaces the cyclone over the western north Pacific, which suppresses local rainfall over the southeastern coast of China. As a result, instead of northerly winds, southwesterly winds contribute to bring water vapor and moisture convergence north to the lower Yangtze region (phase 8 in Fig. 7), benefiting the enhanced rainfall anomaly here and the circulation on and around the TP turns again (phase 8 in Fig. 6).

The SWJS, South Asian high and WNPSH therefore largely account for the zigzag propagation of the QBWO in rainfall. The SWJS and the South Asian high contribute to the anomalous upper level divergence, which favors the occurrence of rainfall in the QBWO anomaly. The SWJS and the South Asian high also act as important guides in the eastward propagation of the QBWO in rainfall. At mid- and lower levels, the east and west shifts in the WNPSH, combining the transition of the circulation over the TP, both play crucial parts in the southward propagation of the QBWO in rainfall. In return, the variations in the SWJS, South Asian high and WNPSH systems may be regulated by the heat source QBWO over the TP. Similar regulatory action takes place in the South China Sea and the western north Pacific (Zhang et al. 2009a, b; Jia and Yang 2013).

### 5 Internal atmospheric dynamic mechanisms for the eastward propagation of rainfall

Figure 6 shows that the positive and negative rainfall in the QBWO anomaly with two large centers over and around the TP have a robust eastward propagation and arrive in central China in phases 1–2 and phases 5–6, respectively. We focus here on the eastward-propagating process to explore the internal atmospheric dynamic mechanisms of this process. We determine whether the mechanisms are different during the two periods of the propagation of

the QBWO on the TP and their spread after leaving the plateau.

The two rainfall centers both clearly correspond to the vertical velocity distribution in the troposphere, accompanying the lower level convergence and upper level divergence shown in Fig. 10a and b. The specific humidity in Fig. 10c shows a clear asymmetrical structure with a higher humidity to the west of 90°E. Figure 10d shows that the eastward movement of the QBWO signals in the rainfall is largely due to the horizontal moisture advection, with the positive horizontal moisture advection to the east of both rainfall centers. The positive horizontal moisture advection favors the convergence of moisture at low levels to the east of the rainfall centers. The vorticity field also shows an asymmetrical structure related to the eastward QBWO with respect to the rainfall centers. A positive vorticity with an equivalent barotropic structure is located to the west of the two centers, especially the first center. Positive horizontal vorticity advection in the upper level appears to the east of the first rainfall center. According to the omega equation in the quasi-geostrophic approximation 
$$-\nabla^2 \omega = f \frac{\partial}{\partial p} \left[ \vec{V}_g \cdot \nabla (f + \zeta_g) \right] - \nabla^2 \left[ \vec{V}_g \cdot \nabla \frac{\partial \phi}{\partial p} \right] - \frac{R}{c_p p} \nabla^2 \frac{dQ}{dt}$$
, the positive vorticity advection increases with height, which easily leads to the occurrence of upward movement and then contributes to the eastward propagation of rainfall in the QBWO anomaly. Hence the positive moisture advection and the vorticity advection both contribute to the eastward propagation of the QBWO in rainfall. However, only the horizontal moisture advection plays a key part in the second eastward-propagating process by promoting the shift in the convergence of moisture at low levels to the east of the rainfall center.

The horizontal moisture advection in the QBWO anomaly can be expressed mathematically as

$$\left( u \frac{\partial q}{\partial x} \right)' \sim -u' \frac{\partial \bar{q}}{\partial x} - \bar{u} \frac{\partial q'}{\partial x}$$

where  $-u' \frac{\partial \bar{q}}{\partial x}$  is the moisture advection due to the mean zonal moisture gradient and  $-\bar{u} \frac{\partial q'}{\partial x}$  is the moisture advection by the mean zonal wind. We investigate which process was more important for the eastward propagation of the QBWO signals. Figure 11a and b clearly show that  $-u' \frac{\partial \bar{q}}{\partial x}$  and  $-\bar{u} \frac{\partial q'}{\partial x}$  contribute to the low-level convergence of moisture to the east of the first and second rainfall centers, respectively. In other words,  $-u' \frac{\partial \bar{q}}{\partial x}$  is more important when the QBWO signals propagate over the TP, whereas  $-\bar{u} \frac{\partial q'}{\partial x}$  plays a key part once the QBWO leaves the TP and continues propagating eastward.

Some of the related meteorological fields can be used to explain the parameters  $-u' \frac{\partial \bar{q}}{\partial x}$  and  $-\bar{u} \frac{\partial q'}{\partial x}$  in detail (Fig. S5). The 10–20-day filtered and raw zonal winds both show

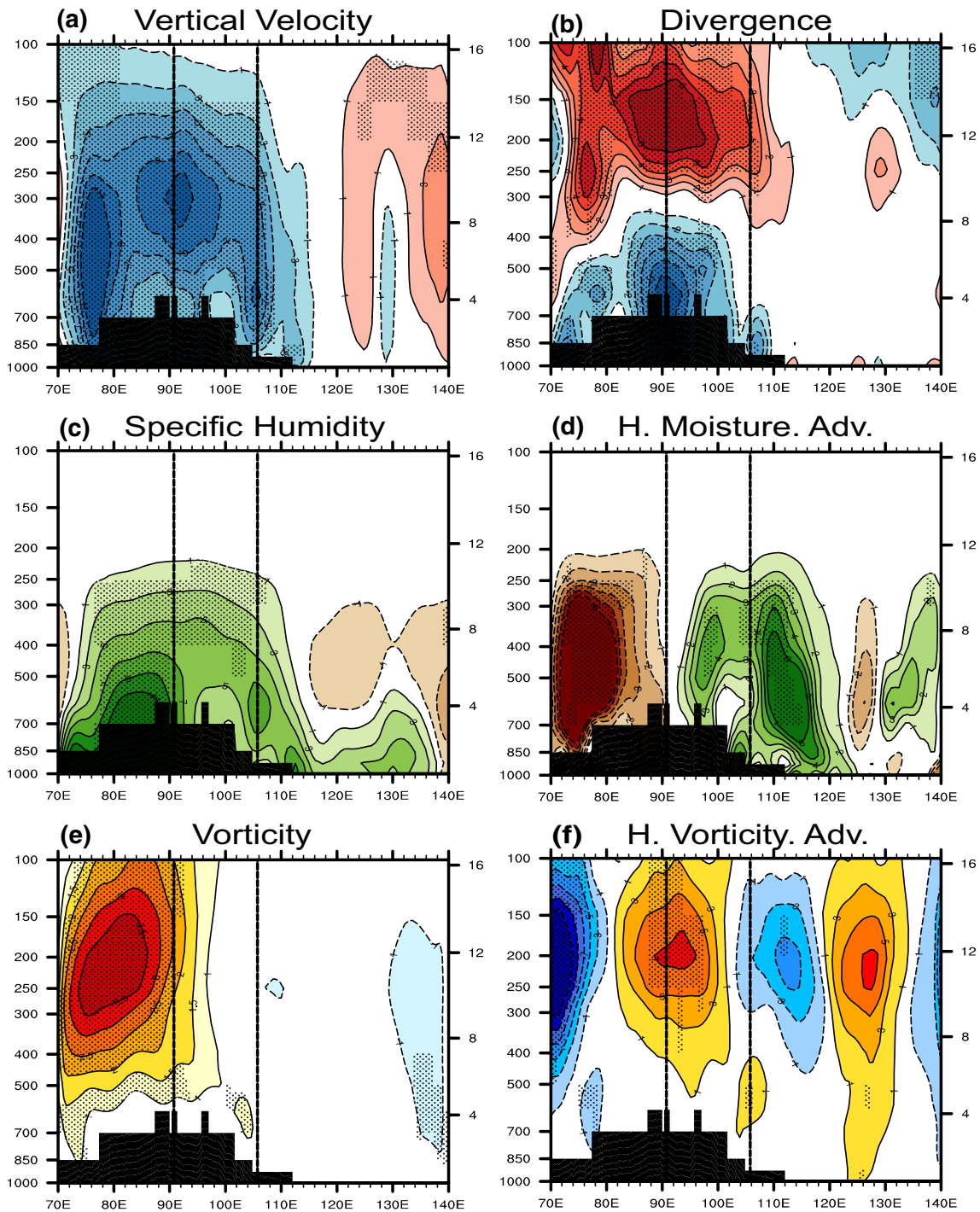


**Fig. 10** Zonal-vertical structures of the eastward-propagating QBWO for **a** vertical velocity ( $10^{-3} \text{ Pa s}^{-1}$ ), **b** divergence ( $10^{-7} \text{ s}^{-1}$ ), **c** specific humidity ( $10^{-5} \text{ kg kg}^{-1}$ ), **d** horizontal moisture advection ( $10^{-10} \text{ kg kg}^{-1} \text{ s}^{-1}$ ), **e** vorticity ( $10^{-6} \text{ s}^{-1}$ ) and **f** horizontal vorticity advec-

tion ( $10^{-11} \text{ s}^{-2}$ ) in phase 1. Shaded areas exceed the 90% confidence level. The two dashed lines represent the two maximum rainfall centers. The vertical axis is the pressure (hPa)

a positive sign with the larger center over the first rainfall center. The parameter  $\frac{\partial \bar{q}}{\partial x}$  shows negative signs to the east of the two rainfall centers, indicating that the signal of  $-u' \frac{\partial \bar{q}}{\partial x}$  is positive. However, the zonal wind in the QBWO anomaly

to the east of the second rainfall center is small (Fig. S5a), which is the main reason why  $-u' \frac{\partial \bar{q}}{\partial x}$  is not clearly seen during the second propagation process (Fig. 11a).  $\frac{\partial q'}{\partial x}$  is also negative to the east of the two rainfall centers, so  $-\bar{u} \frac{\partial q'}{\partial x}$  is

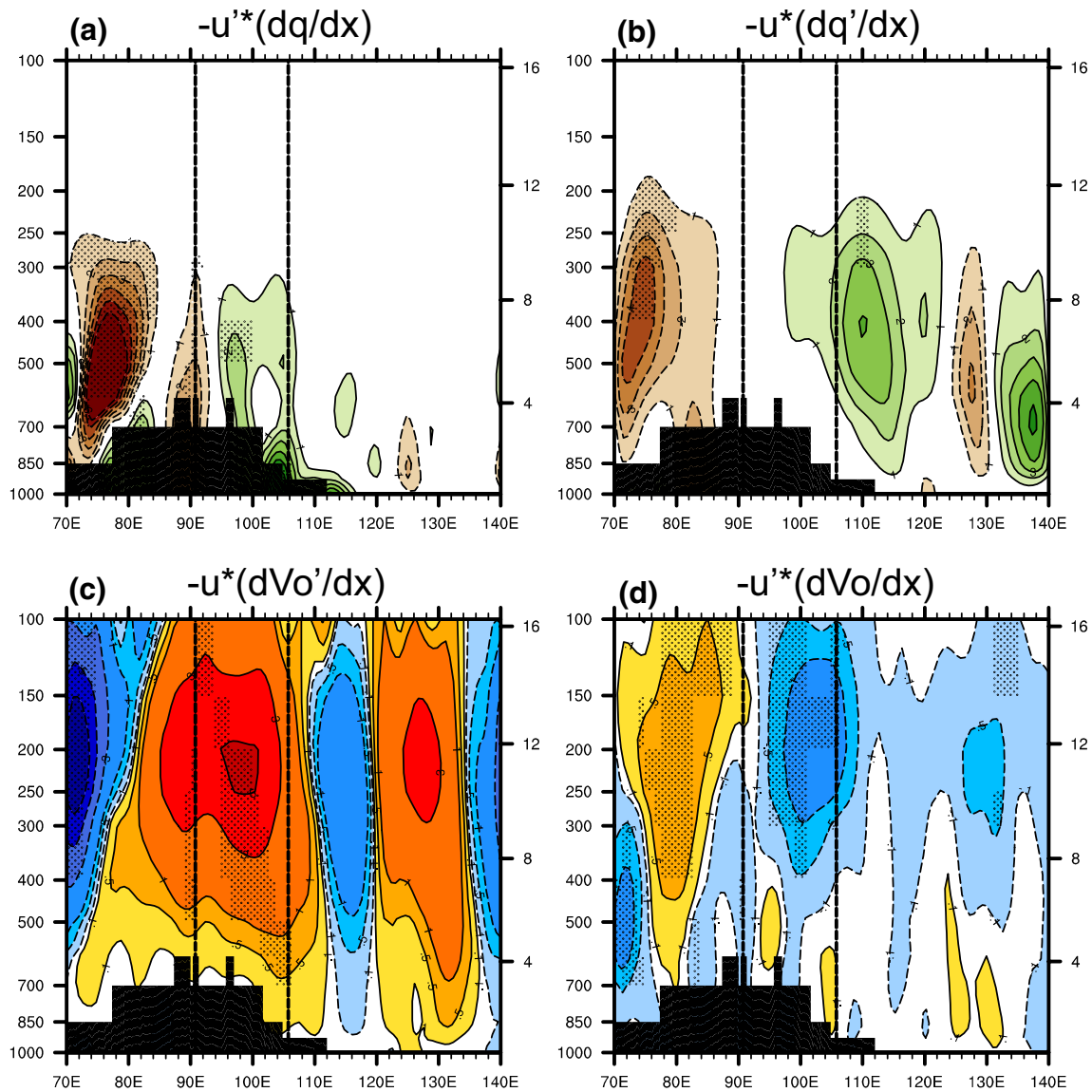


**Fig. 11** As in Fig. 10, but for **a** the horizontal moisture advection due to the mean zonal moisture gradient ( $10^{-10} \text{ kg kg}^{-1} \text{ s}^{-1}$ ), **b** the horizontal moisture advection by the mean zonal wind ( $10^{-10} \text{ kg kg}^{-1}$

$\text{s}^{-1}$ ), **c** the horizontal vorticity advection by the mean zonal wind ( $10^{-11} \text{ s}^{-2}$ ) and **d** the horizontal vorticity advection due to the mean zonal vorticity gradient ( $10^{-11} \text{ s}^{-2}$ )

positive. However, the raw zonal wind and  $\frac{\partial q'}{\partial x}$  to the east of the second rainfall center is larger and more significant than that at the first rainfall center, which explains why  $-\bar{u} \frac{\partial q'}{\partial x}$  is mainly responsible for the eastward movement of the QBWO during the second process (Fig. 11b).

Analogously, the horizontal vorticity advection is composed of  $-u' \frac{\partial \bar{V}_o}{\partial x}$  and  $-\bar{u} \frac{\partial V'_o}{\partial x}$ , which represent the advection of vorticity due to the mean zonal vorticity gradient and the advection of vorticity by the mean zonal wind, respectively. Figure 11c, d clearly show that  $-\bar{u} \frac{\partial V'_o}{\partial x}$  rather than  $-u' \frac{\partial \bar{V}_o}{\partial x}$  contributes to the horizontal vorticity advection.

## 6 Summary and discussion

Using station observations and JRA-55 reanalysis data from 1979 to 2014, we examined the impacts of the atmospheric heating ISV over the TP on summer rainfall in eastern China on an intraseasonal timescale, including the specific pathways, the affected areas and the possible mechanisms (Fig. 12). The main conclusions can be summarized as follows.

1. The dominant ISV over the TP is the QBWO, with another significant 7–9-day oscillation. Summer rain-

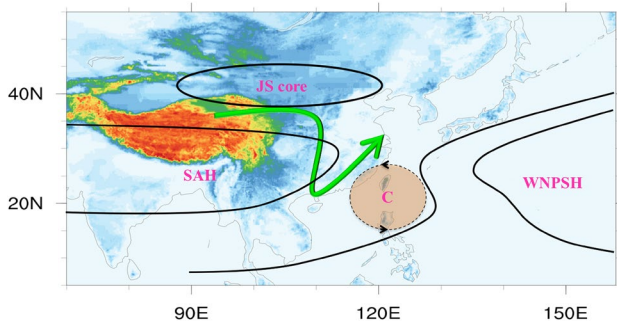


**Fig. 12** Schematic diagram showing the QBWO mode in the atmospheric heat source over the TP, synthesizing the QBWO influence of the TP heat source on summer rainfall in eastern China and the related circulation systems (jet stream core (JC), South Asian high (SAH) and WNPSH) in the upper, mid- and lower levels. The green vector shows the propagation pathway of the QBWO in summer rainfall under the impact of the TP heating QBWO. The letter C represents the cyclone and the adjacent curve is the monsoon trough

fall in eastern China shows a seesaw pattern between central and southern China and the rainfall in these two regions has a common significant periodicity of 10–20 and 7–9 days. The quasi-30-day oscillation is also significant in southern China.

2. The QBWO over the TP has clear eastward-propagating characteristics extending to eastern China. The QBWO over the western TP moves rapidly eastward to the eastern TP with an approximate mean speed of  $6 \text{ m s}^{-1}$ . After moving off the TP, the QBWO has a relatively slow speed of about  $3 \text{ m s}^{-1}$  and continues to propagate toward eastern China.
3. Under the influence of the QBWO over the TP, the East Asian summer rainfall in the QBWO anomaly shows a zigzag, but clear, propagation pathway. An extensive positive rainfall QBWO over and around the TP first shows a robust eastward movement in phase 1 and then controls the region of central China. With a weakening eastward propagation, the QBWO signals move southward to southern China and mix with the signals originating from the southeastern coast of China during phases 3–5. In the following phases, the mixed QBWO signals begin to move northeastward and finally arrive at the lower reaches of the Yangtze River in phase 8. The negative rainfall in the QBWO anomaly repeats the same propagation pathway and continues the circle.
4. In the upper levels of the atmosphere, the SWJS core and South Asian high both gradually move eastward, which strengthens the divergence over East Asia and leads the eastward movement of the QBWO in the positive rainfall. The variation of the WNPSH is significant at mid- and lower levels. When the WNPSH retreats eastward, the QBWO in the geopotential height and the monsoon trough over the western north Pacific decrease and

deepen, respectively, forming an anomalous cyclone. The prevailing northerly to the west of the anomalous cyclone guides the rainfall QBWO originating from the TP southward. A dry phase occupies the TP with northerly winds to the east, which favors the southward propagation of the QBWO in rainfall. The changes are reversed when the WPSH moves westward.

5. The horizontal moisture advection and the horizontal vorticity advection are the two internal atmospheric dynamic mechanisms responsible for the eastward movement of the QBWO in rainfall. When QBWO is moving over the TP, the advection of moisture by the mean zonal wind ( $-\bar{u} \frac{\partial q'}{\partial x}$ ) plays an important part. When the QBWO moves off the TP and continues to move eastward, however, the contribution of the advection of moisture due to the mean zonal moisture gradient ( $-u' \frac{\partial \bar{q}}{\partial x}$ ) plays a major part. With respect to the advection of vorticity,  $-\bar{u} \frac{\partial v'}{\partial x}$  rather than  $-u' \frac{\partial \bar{v}}{\partial x}$  is significant when the QBWO propagates eastward over the TP.

We focused on the influence of the QBWO of the TP heat source regardless of its source. However, based on multi-source and long-term datasets, recent studies (Wang and Duan 2015; Wang et al. 2017, 2018; Yang et al. 2017) have shown that the QBWO signals over the low and mid- to high latitudes contribute to the TP QBWO. In addition, the TP itself also is a center of ISV, with QBWO signals remaining in place locally or spreading to the surrounding areas (Wang and Duan 2015). The mechanisms for the generation and maintenance of the TP local ISV is still a problem. More researches are required to determine the proportion of impacts of the QBWO signals from different sources on the ISV of summer rainfall in eastern China and whether there are differences in the influencing mechanisms.

**Acknowledgements** This work was jointly supported by the National Natural Science Foundation of China (41605039, 91637312, 41807434, 41725018, and 91337218) and the Natural Science Foundation of Jiangsu Province, China (BK20160625). Meirong Wang and Jun Wang thank the China Scholarship Council for funding.

**Open Access** This article is distributed under the terms of the Creative Commons Attribution 4.0 International License (<http://creativecommons.org/licenses/by/4.0/>), which permits unrestricted use, distribution, and reproduction in any medium, provided you give appropriate credit to the original author(s) and the source, provide a link to the Creative Commons license, and indicate if changes were made.

## References

- Bretherton CS, Widmann M, Dymnikov VP et al (1999) The effective number of spatial degrees of freedom of a time-varying field. *J Clim* 12:1990–2009

- Dee DP et al (2011) The ERA-Interim reanalysis: configuration and performance of the data assimilation system. *Quart J R Meteorol Soc* 137:553–597
- Duan AM, Wu GX (2005) Role of the Tibetan Plateau thermal forcing in the summer climate patterns over subtropical Asia. *Clim Dyn* 24:793–807
- Duan AM, Wu GX (2008) Weakening trend in the atmospheric heat source over the Tibetan plateau during recent decades. Part I: observations. *J Clim* 21:3149–3164
- Duan A, Hu J, Xiao Z (2013) The Tibetan plateau summer monsoon in the CMIP5 simulations. *J Clim* 26:7747–7766. <https://doi.org/10.1175/jcli-d-12-00685.1>
- Duchon CE (1979) Lanczos filtering in one and two dimensions. *J Appl Meteor* 18
- Flohn H (1957) Large-scale aspects of the summer monsoon in South and East Asia. *J Meteorol Soc Jpn* 35:180–186
- Flohn H (1960) Recent investigations on the mechanism of the “summer monsoon” of southern and eastern Asia. *Monsoons of the World*, N. Delhi, Ed., Hindu Union Press, 75–88
- Fujinami H, Yasunari T (2001) The seasonal and intraseasonal variability of diurnal cloud activity over the Tibetan Plateau. *J Meteorol Soc Jpn* 79:1207–1227. <https://doi.org/10.2151/jmsj.79.1207>
- Fujinami H, Yasunari T (2004) Submonthly variability of convection and circulation over and around the Tibetan Plateau during the boreal summer. *J Meteorol Soc Jpn* 82:1545–1564. <https://doi.org/10.2151/jmsj.82.1545>
- Fujinami H, Yasunari T (2009) The effects of midlatitude waves over and around the Tibetan plateau on submonthly variability of the East Asian summer monsoon. *Mon Weather Rev* 137:2286–2304. <https://doi.org/10.1175/2009mwr2826.1>
- Gilman DL, Fuglister FJ, Mitchell JM Jr (1963) On the power spectrum of red noise. *J Atmos Sci* 20(2):182–184
- Gong YF, Duan TY, Zhang H (2007) Characteristics of the atmospheric heating source/sink over Asia and its relationship with drought/flood in the Yangtze River-Huaihe River Valley. *Chin J Atmos Sci* 31(1):89–98
- Hsu HH, Liu X (2003) Relationship between the Tibetan Plateau heating and East Asian summer monsoon rainfall. *Geophys Res Lett* 30:D2066
- Hu J, Duan AM (2015) Relative contributions of the Tibetan Plateau thermal forcing and the Indian Ocean Sea surface temperature basin mode to the interannual variability of the East Asian summer monsoon. *Clim Dyn* 45:697–711
- Hu WT, Duan AM, Li Y, He B (2016) The intraseasonal oscillation of Eastern Tibetan plateau precipitation in response to the summer Eurasian wave train. *J Clim* 29:7215–7230. <https://doi.org/10.1175/Jcli-D-15-0620.1>
- Jia X, Yang S (2013) Impact of the quasi-biweekly oscillation over the western North Pacific on East Asian subtropical monsoon during early summer. *J Geophys Res: Atmos* 118:4421–4434. <https://doi.org/10.1002/jgrd.50422>
- Kikuchi K, Wang B (2009) Global Perspective of the Quasi-Biweekly Oscillation. *J Clim* 22:1340–1359. <https://doi.org/10.1175/2008jcli2368.1>
- Kobayashi S et al (2015) The JRA-55 reanalysis: general specifications and basic characteristics. *J Meteorol Soc Japan* 93:5–48
- Krishnamurti TN, Subrahmanyam D (1982) The 30–50 day mode at 850 mb during MONEX. *J Atmos Sci* 39:2088–2095
- Lau WKM (2002) Intraseasonal variability of the atmosphere–ocean–climate system: East Asian monsoon
- Li L, Zhang R (2018) Effect of the atmospheric quasi-biweekly oscillation on the vortices moving off the Tibetan Plateau. *Clim Dyn*. <https://doi.org/10.1007/s00382-017-3672-3>
- Li YK, Sun ZB, Zhang JJ (1991) Relationship between the 30–60 day oscillations in and around the Qinghai-Xizang plateau during the summer half year and the atmospheric circulation. *J Nanjing Inst Meteorol* 14:483–488 (in Chinese)
- Li L, Zhang R, Wen M (2017) Modulation of the atmospheric quasi-biweekly oscillation on the diurnal variation of the occurrence frequency of the Tibetan Plateau vortices. *Clim Dyn* 50:4507–4518. <https://doi.org/10.1007/s00382-017-3887-3>
- Liu FM, Lin H (1991) Relationships between the atmospheric low-frequency oscillation and the variation of the South Asian high. *Plateau Meteorol* 10:61–69 (in Chinese)
- Luo HB, Yanai M (1983) The large-scale circulation and heat sources over Tibetan Plateau and surrounding areas during the early summer of 1979. Part I: precipitation and kinematic analyses. *Mon Wea Rev* 111:922–944
- Luo HB, Yanai M (1984) The large-scale circulation and heat sources over Tibetan Plateau and surrounding areas during the early summer of 1979. Part II: heat and moisture budgets. *Mon Weather Rev* 112:966–989
- Mao JY, Chan JCL (2005) Intraseasonal variability of the South China Sea summer monsoon. *J Clim* 18:2388–2402. <https://doi.org/10.1175/Jcli3395.1>
- Mao JY, Wu GX (2006) Intraseasonal variations of the Yangtze rainfall and its related atmospheric circulation features during the 1991 summer. *Clim Dyn* 27:815–830
- Nitta T (1983) Observational study of heat sources over the eastern Tibetan Plateau during the summer monsoon. *J Meteorol Soc Japan* 61:590–605
- Tao SY, Ding YH (1981) Observational evidence of the influence of the Qinghai-Xizang (Tibet) plateau on the occurrence of heavy rain and severe convective storms in China. *Bull Am Meteorol Soc* 62:23–30
- Wang M, Duan A (2015) Quasi-Biweekly oscillation over the Tibetan Plateau and its link with the Asian summer monsoon. *J Clim* 28:4921–4940. <https://doi.org/10.1175/jcli-d-14-00658.1>
- Wang YN, Chen LX, He JH, Zhang B (2009) Effect of summer heat source low-frequency oscillation over the Tibetan Plateau on precipitation in eastern China. *J Appl Meteorol Sci* 20(4):419–427
- Wang M, Zhou S, Duan A (2011) Trend in the atmospheric heat source over the central and eastern Tibetan Plateau during recent decades: comparison of observations and reanalysis data. *Chin Sci Bull* 57:548–557
- Wang M, Wang J, Duan A (2017) Propagation and mechanisms of the quasi-biweekly oscillation over the Asian summer monsoon region. *J Meteorol Res* 31:321–335. <https://doi.org/10.1007/s13351-017-6131-5>
- Wang M, Wang J, Duan A, Liu Y, Zhou S (2018) Coupling of the quasi-biweekly oscillation of the Tibetan Plateau summer monsoon with the Arctic oscillation. *Geophys Res Lett*. <https://doi.org/10.1029/2018gl077136>
- Wu GX, Zhang YS (1998) Tibetan Plateau forcing and the timing of the monsoon onset over South Asia and the South China Sea. *Mon Weather Rev* 126:913–927
- Wu GX, Liu YM, He B et al (2012) Thermal controls on the Asian summer monsoon. *Sci Rep* 2:404
- Xie A, Ye Q, Chen LX (1989) The atmospheric oscillations over the Tibetan Plateau and surrounding areas as revealed from OLR data. *Acta Meteorol Sin* 47:272–278 (in Chinese)
- Yamada T, Uyeda H (2006) Transition of the rainfall characteristics related to the moistening of the land surface over the central Tibetan Plateau during the summer of 1998. *Mon Weather Rev* 134:3230–3247
- Yanai M (1961) A detailed analysis of typhoon formation. *J Meteorol Soc Jpn* 39:187–214
- Yanai M, Esbensen S, Chu JH (1973) Determination of bulk properties of tropical cloud clusters from large-scale heat and moisture budget. *J Atmos Sci* 30:611–627

- Yang QM (2009) The 20–30-day oscillation of the global circulation and heavy precipitation over the lower reaches of the Yangtze River valley. *Sci China Ser D* 52:1485–1501
- Yang S, Li T (2017) Causes of intraseasonal diabatic heating variability over and near the Tibetan Plateau in boreal summer. *Clim Dyn*. <https://doi.org/10.1007/s00382-016-3463-2>
- Yang J, Wang B, Wang B, Li L (2009) The East Asia-western North Pacific boreal summer intraseasonal oscillation simulated in GAMIL 1.1.1. *Adv Atmos Sci* 26:480–492. <https://doi.org/10.1007/s00376-009-0480-7>
- Yang J, Bao Q, Wang B, He HZ, Gao MN, Gong DY (2017) Characterizing two types of transient intraseasonal oscillations in the Eastern Tibetan Plateau summer rainfall. *Clim Dyn* 48:1749–1768. <https://doi.org/10.1007/s00382-016-3170-z>
- Yang J, Wang W-C, Chen G, Bao Q, Qi X, Zhou S (2018) Intraseasonal variation of the black carbon aerosol concentration and its impact on atmospheric circulation over the Southeastern Tibetan Plateau. *Atmos, J Geophys Res*. <https://doi.org/10.1029/2018jd029013>
- Yasunari T, Miwa T (2006) Convection cloud systems over the Tibetan Plateau and their impact on meso-scale disturbances in the Meiyu/Baiu frontal zone—a case study in 1998. *J Meteorol Soc Jpn* 84:783–803
- Zhang L, Wang BZ, Zeng QC (2009a) Impact of the Madden–Julian oscillation on summer rainfall in Southeast China. *J Clim* 22:201–216
- Zhang Y, Chen LX, He JH (2009b) A study of the characteristics of the low-frequency circulation over the Tibetan Plateau and its association with precipitation in the Yangtze River valley in 1998. *Acta Meteorol Sin* 23:175–190
- Zhang P, Li G, Fu X, Liu Y, Li L (2014) Clustering of Tibetan Plateau vortices by 10–30-day intraseasonal oscillation. *Mon Weather Rev* 142:290–300. <https://doi.org/10.1175/mwr-d-13-00137.1>
- Zhao P, Chen LX (2001) Interannual variability of atmospheric heat source/sink over the Qinghai-Xizang (Tibetan) Plateau and its relation to circulation. *Adv Atmos Sci* 18:106–116
- Zhou B, He JH, Xu HM (2000) LFO characteristics of meteorological elements over Tibetan Plateau and the relations with regional summer rainfall. *J Nanjing Inst Meteor* 23:93–100 (in Chinese)

**Publisher's Note** Springer Nature remains neutral with regard to jurisdictional claims in published maps and institutional affiliations.